

Quantum Dynamical Emulation

Jacob M. Leamer^{1,2}, Denys I. Bondar¹ and Gerard McCaul¹

¹*Tulane University, New Orleans, LA 70118, USA*

²*Quantum Algorithms and Applications Collaboratory,
Sandia National Laboratories, Albuquerque, New Mexico 87185, USA*

(Dated: February 2024)

We introduce the concept of *Quantum Dynamical Emulation*, a constructive method for mapping the solutions of non-unitary dynamics to a weighted set of unitary operations. This allows us to derive a new correspondence between real and imaginary time, which we term Imaginary Time Quantum Dynamical Emulation (ITQDE). This enables an imaginary time evolution to be constructed from the overlaps of states evolved in opposite directions in real time. We show that a single trajectory evolved using ITQDE can be used not only to infer ground and thermal states, but also to resolve information about the complete Hamiltonian spectrum. We further employ ITQDE to derive novel thermodynamic results, including a generalisation of the Hubbard-Stratonovich transform. We go on to develop a quantum algorithm for computing the spectra of quantum systems that is based on this premise. We demonstrate the utility of this method through numerical simulation, as well as quantum hardware implementations.

I. INTRODUCTION

Few mathematical concepts have furthered our understanding of the real to a greater degree than the imaginary. From its first use in the solution of cubic polynomials, the introduction of imaginary numbers dramatically expands the scope of both the solvable and conceivable. In the domain of physics, the alchemy of i has an enduring capacity to surprise. For example, the Wick rotation [1] is celebrated as a tangible link between statistical mechanics and quantum dynamics, where oscillation is transformed to decay. In this sense, evolution in imaginary time might rightly be thought of as the dynamics of equilibration.

This equilibrium information, and methods to obtain it, are perhaps the overriding preoccupation of physics. Beyond the ground state, the spectral gap is also of fundamental interest due to its role in phase transitions [2–6], as well as in quantum information [7]. As such, there has been a great deal of interest in developing methods for determining excited states [8–19]. Moreover, with the discovery of dynamical phase transitions an open question has arisen as to how these relate to the system equilibrium. Furthermore, in the regime of quantum chaos, a parallel question arises as to whether the signatures of chaotic dynamics can be found in a system’s spectral characteristics [20, 21].

Imaginary time evolution is a powerful method for obtaining equilibrium information about a quantum system, and is used extensively in computational methods such as quantum Monte Carlo. The premise is that, as a quantum state is evolved in imaginary time τ , higher energy states decay exponentially faster than lower energy states. As long as the system has some initial support on the ground state, then in the limit of large τ , the system converges to the ground state.

Ground state calculations are of course central to numerous applications [22–24], e.g., in solid state physics and quantum chemistry [25–28], but with suitable inter-

pretation of the Hamiltonian, can also represent solutions to computational problems. Beyond ground states, imaginary time evolution can also be used to calculate thermal states, also known as Gibbs states, at finite temperatures [29–31]. Such states are crucial in a wide range of inquiry, ranging (naturally) from the thermalization of quantum systems [32–36] to efficient optimization procedures [37, 38].

While imaginary time evolution is a celebrated technique across multiple computational methods, it does not map naturally to quantum computers, which are widely hoped to advance our ability to perform difficult simulations of quantum systems [39, 40]. This is because algorithms for typical, circuit-model quantum computers are constructed using quantum logic gates, which are unitary operations, while imaginary time evolution is not a unitary process. Nevertheless, for the reasons outlined above, there has been intense interest in adapting this powerful method to quantum algorithms [41–47]. Thus far, these methods rely either on variational methods to approximate the non-unitary operation of imaginary time [48], or probabilistic approaches [49]. In both cases, the non-constructive nature of these techniques manifests itself in undesirable features. For example Quantum Imaginary Time Evolution (QITE) requires unitary operations on a scaling domain of qubits [48], while Probabilistic Imaginary Time Evolution (PITE) [49] exhibits an exponential decrease in success probability as one evolves further into imaginary time.

The apparent incompatibility of imaginary time simulations with the building blocks of circuit-model quantum computation also speaks to a broader challenge: our ability to manipulate physical systems is stranded in real time, while the ultimate answers to the questions we seek to ask can be most transparently sought with the use of non-unitary dynamics. Any result able to constructively represent such non-unitary dynamics in terms of unitary operations would constitute a novel tool for the exploration of the topics outlined above.

Here, we propose a new approach to this problem, and others, which we term *Quantum Dynamical Emulation* (QDE). As outlined above, for reasons both of aesthetics and practical importance, we choose to apply it first to the emulation of imaginary time evolutions, terming this specification of QDE *Imaginary Time Quantum Dynamical Emulation* (ITQDE). As a first application we employ it in the implementation of spectral calculations in quantum circuits, but emphasise that the methods pioneered by QDE are likely to find useful application in a wide variety of contexts. Using ITQDE, we specifically demonstrate that expectation values of a state evolved in imaginary time can be expressed in terms of the overlaps of states that are propagated forwards and backwards in real time.

Unlike the aforementioned quantum algorithms, which aim at generating imaginary time in a quantum circuit, ITQDE is a constructive, deterministic approach that is consequently applicable to a much broader context, and which establishes novel links between unitary evolutions and *Gaussian* - rather than Gibbs - states. It is established without requiring any reference to algorithmic results, and yields a number of surprising links between physical and thermalising dynamics. In particular ITQDE recovers in its continuum limit a result fundamental to stochastic and quantum thermodynamics - the Hubbard-Stratonovich transformation, offering a new interpretation of its origin in the process. Not only this, ITQDE is *also* of a form manifestly implementable in the current circuit-model paradigm for quantum computation, possessing the significant conceptual advantage that it relies on no variational or probabilistic arguments, and - at most - only a single ancilla qubit. We use this fact to demonstrate ITQDE can be leveraged to perform sampling-based spectral calculations of correlated materials in quantum computers.

The remainder of the paper is organised as follows. We begin by expounding the underlying philosophy of QDE in Sec. II, before applying it to derive the ITQDE correspondence for representing imaginary time-like dynamics in terms of unitary operations. The analytical and numerical properties of the technique are also discussed, together with its continuous limit. We then extend the derived correspondence in Sec. III to develop a technique for resolving spectral information from dynamical overlaps. Following this, in Sec. IV we sketch several potential applications of ITQDE in the realm of thermodynamics. Sec. V then provides numerical illustrations of ITQDE resolving the spectra of correlated materials. A first experimental result utilising this correspondence is then presented in Sec. VI, where a quantum algorithm for implementing ITQDE is detailed, together with the results obtained from its execution in both simulation and hardware. We then close the paper with a discussion of further future applications and generalisations of this work in Sec. VII.

II. LINKING REAL AND IMAGINARY EVOLUTIONS WITH QUANTUM DYNAMICAL EMULATION

At root, QDE exploits a freedom in the interpretation of a set of unitary operations applied to a state ρ . We first define a superoperator

$$\mathcal{L}[\rho] = \sum_{ij} k_{ij} \mathcal{U}_i \rho \mathcal{U}_j \quad (1)$$

where k_{ij} are weights on the application of some set of unitary operations $\{\mathcal{U}_j\}$. We note immediately that in general this need not conform to the form of a Kraus map, and in such a case is not trace-preserving and therefore not *directly* physical. Nevertheless this operation is composed purely of unitary operations on states, which are individually implementable in a physical context. As we shall see, this allows one to ultimately interpret the action of this operation as being equivalent to an averaging over physically realisable unitary evolutions. This is the heart of QDE, enabling constructive unitary representations of non-unitary dynamics.

To make this connection, we first stipulate our set of unitaries are parametrised by some increment $\Delta\tau$ (or fractional powers of that increment). This allows for the interpretation of $\mathcal{L}[\rho]$, as a infinitesimal generator for a differential equation. Specifically, $\mathcal{L}[\rho]$ can be Taylor expanded to the form:

$$\mathcal{L}[\rho] = \rho + \Delta\tau \mathcal{G}[\rho] + \mathcal{O}(\Delta\tau^2), \quad (2)$$

such that $\mathcal{L}^m[\rho]$ corresponds to a state that is the solution to the differential equation

$$\frac{d}{d\tau} \tilde{\rho}(\tau) = \mathcal{G}[\tilde{\rho}(\tau)] \quad (3)$$

for $\tau = m\Delta\tau$.

Surprisingly, it is relatively easy to choose $\{\mathcal{U}_j\}$ such that this differential equation is explicitly of a non-unitary character. Indeed, if Eq. (1) is not of the Kraus form then the evolution is not trace preserving and the resulting state definitionally cannot be obtained unitarily. The result of this differential equation is approximately equivalent to m repeated applications of this superoperator $\mathcal{L}^m[\rho]$, i.e., $\rho_m = \mathcal{L}^m[\rho]$. While $\mathcal{L}^m[\rho]$ is not directly implementable, it can after normalisation be interpreted as an *average* of physically realisable unitary operations of states. In this regard, $\mathcal{L}^m[\rho]$ is realisable as a set of unitary operations which, in combination, correspond to a state that is not otherwise directly accessible by such operations. The approximate equating of the two states ρ_m and $\tilde{\rho}(\tau)$ establishes QDE as a constructive method for unitary representations of non-unitary dynamics and is schematically represented in Fig. 1.

QDE may rightly be thought of as a spiritual successor to Ensemble Rank Truncation [50] and corner space techniques [51–53], where it was conceived of as an efficient deterministic method for the simulation of Lindblad equations. QDE greatly extends this idea, however, to capture more general dynamics. This is most

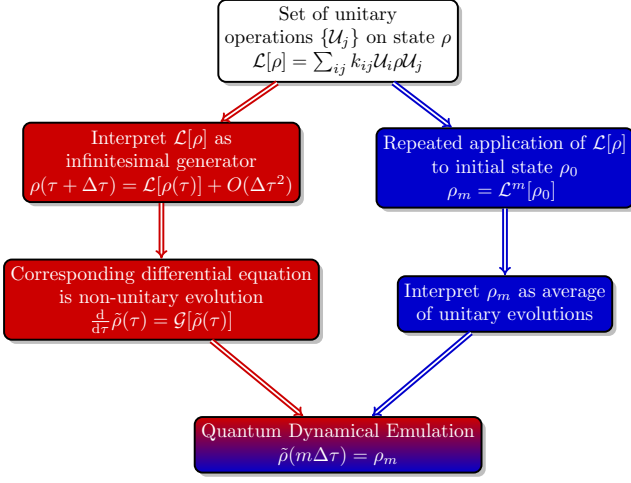


FIG. 1. Schematic illustration of Quantum Dynamical Emulation (QDE). The action of a set of unitary operations on a state has an alternative interpretation as a generator for differential equation. Depending on the chosen form of $\{\mathcal{U}_j\}$, this may be a non-unitary evolution. QDE equates the result of such a non-unitary evolution to the unitary operation $\mathcal{L}^m[\rho]$.

easily demonstrated by outlining QDE's application to the problem of unitary representations of imaginary-time evolved states. We begin with the unitary

$$\mathcal{U} = e^{-i\sqrt{\frac{\Delta\tau}{2}}H}, \quad (4)$$

which represents evolution in real time under a Hamiltonian H for a time $\sqrt{\frac{\Delta\tau}{2}}$. With this, we define the superoperator

$$\mathcal{L}[\rho] = \frac{1}{2} (\mathcal{U}\rho(\tau)\mathcal{U} + \mathcal{U}^\dagger\rho(\tau)\mathcal{U}^\dagger), \quad (5)$$

whose effect at first order in $\Delta\tau$ is given by

$$\mathcal{L}[\rho] = \rho - \frac{\Delta\tau}{4} (\{\rho, H^2\} + 2H\rho H) + \mathcal{O}(\Delta\tau^2), \quad (6)$$

where $\{\cdot, \cdot\}$ denotes the anticommutator. From Eq. 6, we observe that for $\Delta\tau \rightarrow 0$, $\mathcal{L}[\rho]$ corresponds to an infinitesimal evolution of ρ according to

$$\frac{d\rho}{d\tau} = -\frac{1}{4} (\{\rho, H^2\} + 2H\rho H), \quad (7)$$

whose (unnormalized) solution is given by

$$\rho(\tau) = \sum_{ij} e^{-\frac{1}{4}\tau(E_i+E_j)^2} p_{ij}(0)|E_i\rangle\langle E_j|. \quad (8)$$

In Eq. 8, $\rho(\tau)$ is expressed in the eigenbasis of the Hamiltonian $H = \sum_i E_i|E_i\rangle\langle E_i|$ with general initial condition $\rho(0) = \sum_{ij} p_{ij}(0)|E_i\rangle\langle E_j|$.

In the limit of large τ , the dominant contribution in $\rho(\tau)$ will be the eigenstate of H with the smallest squared eigenvalue, i.e.,

$$\rho(\tau) \rightarrow e^{-\tau E_\ell^2} p_{\ell\ell}(0)|E_\ell\rangle\langle E_\ell| \quad (9)$$

for $\tau \rightarrow \infty$, where $E_\ell^2 = \min_j E_j^2$ is the ground state energy of H^2 . Other matrix elements of $\rho(\tau)$ will be exponentially suppressed in τ according to Eq. 8.

The result in Eq. 9 is directly analogous to the outcome of evolving the state $\rho(0)$ in *imaginary time* under the Hamiltonian H^2 , and could accordingly be used to study ground states of H^2 via Eq. (9). However, we emphasize that we have obtained Eq. 9 utilizing purely unitary, real-time evolutions per Eq. 5.

Having obtained Eq. (8), we now consider the repeated application of Eq. 5, denoting m applications of \mathcal{L} by $\mathcal{L}^m[\rho]$. We consider an initial condition that is given by the pure state

$$\rho(0) = |\psi_0\rangle\langle\psi_0|, \quad (10)$$

noting that the generalization to mixed states is straightforward. Introducing the following notation for forwards and backwards evolved states,

$$|\psi_{j+1}\rangle = \mathcal{U}|\psi_j\rangle, \quad |\psi_{j-1}\rangle = \mathcal{U}^\dagger|\psi_j\rangle, \quad (11)$$

a single application of \mathcal{L} yields

$$\rho(\Delta\tau) = \mathcal{L}[\rho(0)] = \frac{1}{2} (|\psi_1\rangle\langle\psi_{-1}| + |\psi_{-1}\rangle\langle\psi_1|). \quad (12)$$

The effect of repeated applications of \mathcal{L} can then be ascertained inductively. Namely, after m steps, $\rho(m\Delta\tau)$ may be written as

$$\rho(m\Delta\tau) = \mathcal{L}^m[\rho(0)] = \sum_{j=0}^{2m} a_j^{(m)} |\psi_{j-m}\rangle\langle\psi_{m-j}|, \quad (13)$$

where the $a_j^{(m)}$ denote coefficients that remain to be calculated. These coefficients have two important properties: first, $a_0^{(m)} = a_{2m}^{(m)} = 1$, and second, the lack of a static term in \mathcal{L} guarantees $a_j^{(m)} = 0$ for odd j .

Applying \mathcal{L} again to Eq. (13), we obtain

$$2\mathcal{L}^{m+1}[\rho(0)] = \sum_{j=0}^{j=2m} a_j^{(m)} (|\psi_{j-(m+1)}\rangle\langle\psi_{m+1-j}| + |\psi_{j+1-m}\rangle\langle\psi_{m-1-j}|). \quad (14)$$

Rearranging indices, we find

$$2\mathcal{L}^{m+1}[\rho(0)] = |\psi_{-m-1}\rangle\langle\psi_{m+1}| + |\psi_{m+1}\rangle\langle\psi_{-m-1}| + \sum_{j=2}^{j=2m} (a_j^{(m)} + a_{j-2}^{(m)}) |\psi_{j-(m+1)}\rangle\langle\psi_{m+1-j}|. \quad (15)$$

This yields the following recursion relation

$$2a_j^{(m+1)} = a_j^{(m)} + a_{j-2}^{(m)}, \quad (16)$$

whose solution is given by Pascal's identity

$$\binom{m}{k} = \binom{m-1}{k} + \binom{m-1}{k-1}, \quad (17)$$

yielding

$$a_j^{(m)} = \begin{cases} \frac{1}{2^m} \binom{m}{\frac{j}{2}} & j \text{ even,} \\ 0 & j \text{ odd.} \end{cases} \quad (18)$$

Using $\tau = m\Delta\tau$, we substitute Eq. 18 into Eq. 13 to finally obtain

$$\rho(\tau) = \frac{1}{2^m} \sum_{j=0}^{j=m} \binom{m}{j} |\psi_{2j-m}\rangle \langle \psi_{m-2j}|. \quad (19)$$

Eq. (19) can be used to simulate the evolution of an initial state $\rho(0)$ in imaginary time under H^2 using only unitary operations, and thus enables what we term *Imaginary Time Quantum Dynamical Emulation* (ITQDE). The error between Eq. (19) and the continuous-time limit given previously in Eq. (8) is $\mathcal{O}(m\Delta\tau^2)$. In the interests of concision, we do not explicitly retain this error term in the sections that follow, but stress that that ITQDE as presented is contingent on this discrete approximation. The continuous limit of ITQDE of this approximation is addressed in Sec. IV.

In many cases, it is desirable to additionally enforce that the state is normalized at all (imaginary) times. This can be accomplished by introducing the partition function, which we denote by $Z(\tau) = \text{Tr}(\rho(\tau))$. We denote the normalized state by $\bar{\rho}(\tau) \equiv \frac{\rho(\tau)}{Z(\tau)}$. With this normalization, we can express the expectation value of an observable, O , under the state $\bar{\rho}(\tau)$ as

$$\langle O \rangle(\tau) = \frac{1}{2^m Z(\tau)} \sum_{j=0}^{j=m} \binom{m}{j} \langle \psi_{2j-m} | O | \psi_{m-2j} \rangle, \quad (20)$$

where

$$Z(\tau) = \frac{1}{2^m} \sum_{j=0}^{j=m} \binom{m}{j} \langle \psi_{2j-m} | \psi_{m-2j} \rangle, \quad (21)$$

noting that when substituting Eq. (21) into Eq. (20), the factors of 2^m cancel.

Equations (20) and (21) illustrate that an observable expectation value with respect to the imaginary time evolved state $\bar{\rho}(\tau)$ is expressible as a weighted sum of overlaps between states that have been evolved unitarily in opposite directions in real time. In order to estimate the expectation value of an observable under the ground state, $|E_\ell\rangle$, of H^2 , one could utilize Eq. (20) carried out to large τ , in line with Eq. (9), where $\rho(0)$ can be any state with nonzero support on $|E_\ell\rangle$.

Large m limit

In settings where many time steps are needed to achieve convergence (i.e., the large m limit), evaluating Eqs. (20) and (21) can be computationally challenging due to the presence of the binomial coefficients $\binom{m}{j}$, whose magnitudes increase very quickly with m . As a practical matter, this challenge can be addressed by first shifting the summation index to make the symmetric nature of the sum explicit, i.e., replacing $\sum_{j=0}^{j=m} \binom{m}{j}$ by $\sum_{j=-\frac{m}{2}}^{\frac{m}{2}} \binom{m}{\frac{m}{2}+j}$ in Eqs. (20) and (21), and then considering the large m asymptotic for the binomial coefficient

$$\binom{m}{m/2+j} \sim \frac{2^m}{\sqrt{m\pi/2}} e^{-2j^2/m}. \quad (22)$$

Henceforth, we assume m to be even. This expression is readily derivable from the Stirling approximation [54], with an error on the order $\mathcal{O}(j^3 m^{-2})$, although as a practical matter this error becomes negligible even for relatively small values of m . Substituting Eq. (22) into Eqs. (20) and (21) yields

$$\langle \tilde{O} \rangle(\tau) = \frac{1}{\tilde{Z}(\tau)} \sum_{j=0}^{j=\frac{m}{2}} \frac{e^{-\frac{2j^2}{m}}}{\sqrt{m\pi/2}} \langle \psi_{2j} | O | \psi_{-2j} \rangle + \text{c.c.} \quad (23)$$

and

$$\tilde{Z}(\tau) = \frac{1}{\sqrt{m\pi/2}} \sum_{j=0}^{j=\frac{m}{2}} e^{-\frac{2j^2}{m}} \langle \psi_{2j} | \psi_{-2j} \rangle + \text{c.c.}, \quad (24)$$

where we use the tilde to denote that the large m approximation has been used. Equations (23) and (24) can be used as alternative equations when m becomes large.

Maximally mixed initial condition

Finally, in the case where the initial condition is given by the identity $\rho(0) = I$, a number of further results can be inferred from ITQDE. This initial condition corresponds to the maximally mixed or infinite temperature state. Beginning from this condition means that at all τ H^2 and ρ necessarily commute, simplifying Eq. (7) such that we obtain at time τ the Gaussian state

$$\rho(\tau) = e^{-\tau H^2}, \quad (25)$$

which is equivalent to a thermal (Gibbs) state with an effective Hamiltonian H^2 at inverse temperature $\beta = \tau$ [55, 56]. This illustrates that in this setting, evolving $\rho(0) \propto 1$ under Eq. (7) is functionally equivalent to imaginary time propagation under H^2 . This suggests that it is desirable to consider this initial condition, given its natural relationship to thermal states.

Furthermore, given $\rho(0) = I$, the final (unnormalized) state in Eq. (19) becomes

$$\rho(\tau) = \frac{1}{2^m} \sum_{j=0}^{j=m} \binom{m}{j} e^{-i(2j-m)\sqrt{2\Delta\tau}H} \quad (26)$$

where the approximation error between Eq. (26) and the Gaussian state solution given in Eq. (25) is also $\mathcal{O}(m\Delta\tau^2)$. In this setting, Eq. (20) can be used to estimate the expectation values of observables under thermal states associated with inverse temperature $\beta = \tau$.

III. ITQDE FOR SPECTRAL CALCULATIONS

We now detail how the ITQDE correspondence can be used to perform spectral calculations. We first observe that when $O = H^2$, evaluating Eq. 20 for large τ would output an estimate of its ground state energy E_ℓ^2 . Similarly, eigenenergies can be estimated with respect to the thermal state described by Eq. (25). To calculate these at some desired inverse temperature β one need only implement Eq. (20) to $\tau = \beta$ from an initial condition of $\rho(0) = \frac{1}{Z(0)}I$.

It is however possible to go further, and exploit ITQDE to perform full spectral calculations that additionally resolve excited states. To demonstrate this, we first note that for a d -dimensional system, there are 2^d possible Hamiltonians H_κ that square to the same H^2 . In other words, for all Hamiltonians H_κ , parameterized by length- d binary strings κ with elements $\kappa_j \in \{0, 1\}$ such that

$$H_\kappa = \sum_{j=0}^{d-1} (-1)^{\kappa_j} E_j |E_j\rangle\langle E_j|, \quad (27)$$

we have that the squares of all these H_κ are identically given by

$$H^2 = \sum_{j=0}^{d-1} E_j^2 |E_j\rangle\langle E_j|. \quad (28)$$

This reinforces that as $\tau \rightarrow \infty$, $\rho(\tau)$ will select the eigenstate of H with the smallest squared eigenvalue per Eq. (9). We can take advantage of this behavior by introducing a shift λ into the Hamiltonian such that

$$H^{(\lambda)} = H + \lambda I. \quad (29)$$

This shift allows one to directly tune which eigenstate has the lowest squared eigenvalue, and accordingly, which eigenstate $\rho^{(\lambda)}(\tau)$ approaches as the system is evolved to higher τ [57]. Importantly, the effect of this shift on \mathcal{U} is simply to introduce a global phase of $e^{-i\sqrt{\frac{\Delta\tau}{2}}\lambda}$, i.e., such that $\mathcal{U}^{(\lambda)} \equiv e^{-i\sqrt{\frac{\Delta\tau}{2}}H^{(\lambda)}} = e^{-i\sqrt{\frac{\Delta\tau}{2}}\lambda} e^{-i\sqrt{\frac{\Delta\tau}{2}}H}$. Given

this, we may describe the expectation value of an observable O with respect to $\rho^{(\lambda)}(\tau)$ as

$$\begin{aligned} \langle O^{(\lambda)} \rangle(\tau) &= \frac{1}{Z^{(\lambda)}(\tau)} \sum_{j=0}^{\frac{m}{2}} \frac{e^{2i\lambda j\sqrt{\frac{\Delta\tau}{2}}}}{2^m} \binom{m}{\frac{m}{2} + j} \langle \psi_{2j} | O | \psi_{-2j} \rangle \\ &+ \text{c.c.}, \end{aligned} \quad (30)$$

where

$$Z^{(\lambda)}(\tau) = \frac{1}{2^m} \sum_{j=0}^{\frac{m}{2}} e^{2i\lambda j\sqrt{\frac{\Delta\tau}{2}}} \binom{m}{\frac{m}{2} + j} \langle \psi_{2j} | \psi_{-2j} \rangle + \text{c.c.}, \quad (31)$$

and we have exploited the fact that each overlap has a conjugate partner to reduce the number of terms in the sums from m to $\frac{m}{2}$.

Meanwhile, in the large m limit we obtain

$$\begin{aligned} \langle \tilde{O}^{(\lambda)} \rangle(\tau) &= \frac{1}{\tilde{Z}^{(\lambda)}(\tau)} \sum_{j=0}^{\frac{m}{2}} \frac{e^{-\frac{2j^2}{m} + 2i\lambda j\sqrt{\frac{\Delta\tau}{2}}}}{\sqrt{m\pi/2}} \langle \psi_{2j} | O | \psi_{-2j} \rangle \\ &+ \text{c.c.} \end{aligned} \quad (32)$$

and

$$\tilde{Z}^{(\lambda)}(\tau) = \frac{1}{\sqrt{m\pi/2}} \sum_{j=0}^{\frac{m}{2}} e^{-\frac{2j^2}{m} + 2i\lambda j\sqrt{\frac{\Delta\tau}{2}}} \langle \psi_{2j} | \psi_{-2j} \rangle + \text{c.c.}, \quad (33)$$

by substituting Eq. (22) into Eqs. (30) and (31).

Crucially, when $O = H$, varying the value of λ allows us to calculate the entire energy spectrum by simply measuring the overlaps $\langle \psi_{2j} | H | \psi_{-2j} \rangle$ and $\langle \psi_{2j} | \psi_{-2j} \rangle$, $j = 0, \dots, m/2$ corresponding to a single trajectory in τ , and then evaluating Eq. (30) for different values of λ as a numerically trivial post-processing step. We also note parenthetically here that for the ground state specifically λ can also be used to accelerate convergence. More details regarding this use are located in App. A.

Somewhat amusingly (and certainly unintentionally), ITQDE implements what has been a long-standing proposal in the context of Monte-Carlo methods [58]. Namely the spectral sweeping enabled by sampling H^2 . Previous efforts in this context have however foundered on the fact that H^2 is not only far more singular than H for any realistic Hamiltonian, but cannot guarantee non-negative weights on paths [59]. The fact that ITQDE never actually employs H^2 in its calculation of spectra raises the possibility that such issues may also be avoided in a Monte-Carlo context.

Finally, we note that ITQDE's ability to resolve spectra is a direct consequence of the imaginary time evolution it implements generating a Gaussian, rather than thermal (or Gibbs) state. In the case that one seeks to obtain the thermal state directly via ITQDE, it is necessary to obtain the 'square root' of the Hamiltonian \sqrt{H} . While we do not address this in the present work, such an operator will always exist for positive semi-definite H

(which can itself be guaranteed with a suitable shift of the spectrum), and quantum algorithmic techniques have already been proposed for the calculation of \sqrt{H} [60].

IV. THERMODYNAMIC APPLICATIONS OF ITQDE

Beyond spectral calculations, the character of the ITQDE correspondence has a number of interesting properties that are worth commenting on. In particular, the presence of forward and reverse trajectories in the correspondence ought not to be ignored, given the ubiquity of this feature in both quantum [61] and stochastic [62] thermodynamics. In the latter case fluctuation theorems are derived from considerations of the probability of trajectories against their reversed counterpart [63], suggesting similar results may be obtained via the methods outlined in previous sections. Indeed, if one were to employ the large m approximation according to Eq. (22), the result

$$e^{-\tau H^2} = \frac{1}{\sqrt{\pi}} \sum_{j=-\frac{m}{2}}^{\frac{m}{2}} \sqrt{\frac{2}{m}} e^{-\frac{2j^2}{m}} e^{-2ij\sqrt{2\Delta\tau}H} \quad (34)$$

can be used to take the expectation of the operator $e^{-\tau H^2}$ with respect to $|\psi_0\rangle$. From this we directly obtain (reiterating the implicit $\mathcal{O}(m\Delta\tau^2)$ error)

$$\langle e^{-\tau H^2} \rangle = \sqrt{\frac{2}{m\pi}} \sum_{j=0}^{\frac{m}{2}} e^{-\frac{2j^2}{m}} \langle \psi_{2j} | \psi_{-2j} \rangle + \text{c.c.}, \quad (35)$$

a result that bears a remarkable similarity to the Crooks fluctuation theorem [64], where the work distribution function of a stochastic process can be expressed as a ratio of the probabilities for forward and reversed processes. In the current instance, we find the expected Hamiltonian Gaussian distribution of a state is expressible in terms of an exponentially weighted sum of *overlaps* between forward and backward evolutions from that state. Indeed, the ITQDE derived expression is a manifestly quantum one, insofar as it utilises overlaps rather than probabilistic ratios, and that it links to distributions over H , rather than the non-observable work variable.

More broadly, it is interesting to observe the tension between microscopic reversibility and thermal equilibration manifest itself here, in the sense that ITQDE suggests that equilibrium properties are the product of *both* forwards and reversed trajectories, rendering the question of directionality redundant. The direction of the arrow of time hardly matters when its consequences are manifestly symmetric. Moreover, given the only sense in which a time increment appears is $\Delta\tau$ - which in the real time propagation occurs under a square root, the notion of time reversal is most naturally captured by the equivalent transformation of $H \rightarrow -H$. Note however that when we consider this transformation in the case

of Gibbs states - the physical thermal distribution - the necessity of employing \sqrt{H} in the propagator means this reversal symmetry is broken. This fact, to the philosophically inclined, may be of some interest.

It is also possible to *invert* the ITQDE correspondence. First, taking the same large m approximation of Eq. (34) and inserting λ , we have:

$$e^{-\tau(H-\lambda)^2} = \frac{1}{\sqrt{\pi}} \sum_{j=-\frac{m}{2}}^{\frac{m}{2}} \sqrt{\frac{2}{m}} e^{-\frac{2j^2}{m}} e^{-2ij\sqrt{2\Delta\tau}H} e^{-2ij\sqrt{2\Delta\tau}\lambda}. \quad (36)$$

Following this, we note the orthogonality relationship for complex exponentials is given by:

$$\sum_{\lambda=0}^{\lambda=K-1} e^{\frac{2i\pi\lambda}{K}(j-k)} = K\delta_{jk}. \quad (37)$$

Let us say that $\frac{m}{2}$ is a square number, such that $K = \sqrt{\frac{m}{2}}$ is an integer. This also means that $K\sqrt{2\Delta\tau} = \sqrt{\tau}$. Then, applying the complex exponential and summing over λ on both sides, we have

$$\sum_{\lambda=0}^{\lambda=K-1} e^{-\tau(H-\frac{\pi}{\sqrt{\tau}}\lambda)^2} e^{\frac{2i\pi\lambda k}{K}} = \frac{1}{\sqrt{\pi}} e^{-\frac{2k^2}{m}} e^{-2ik\sqrt{2\Delta\tau}H}. \quad (38)$$

By defining $t = 2k\sqrt{2\Delta\tau}$ and rearranging, we obtain an expression for the propagator:

$$e^{-itH} = \sqrt{\pi} e^{\frac{t^2}{4\tau}} \sum_{\lambda=0}^{\lambda=K-1} e^{-\tau(H-\frac{\pi}{\sqrt{\tau}}\lambda)^2} e^{\frac{2i\pi\lambda t}{\sqrt{\tau}}}. \quad (39)$$

The fundamental motivation for such a representation is that it allows one to cast dynamical processes purely in terms of equilibrium information, with time acting only as a weighted phase on shifted Gaussian distributions. This expression may therefore likely be useful in obtaining alternate formulations of dynamical quantities such as a system's dynamic response [65] or Out-Of-Time-Order Correlators (OTOCs) [66]. This latter quantity is a measure of information scrambling, and recent proposals have demonstrated its intrinsic relationship to thermodynamics [67]. In this sense Eq.(39) offers a natural route to further exploration of this connection. Moreover, in the context of both OTOCs and Lyapunov exponents, a t^2 exponent often emerges, identical to that obtained in the inverted ITQDE correspondence above. Such coincidences are suggestive of deeper links that might be uncovered with a systematic application of ITQDE to these topics.

Lastly, if we consider the continuous limit of Eq. (26), a further connection to open systems theory is revealed. Returning to Eq. (34) and defining $\delta = \sqrt{\frac{2}{m}}$ and $x = j\delta$, the right-hand-side of Eq. (34) may be expressed as

$$e^{-\tau H^2} = \frac{1}{\sqrt{\pi}} \sum_{j=-\frac{m}{2}}^{\frac{m}{2}} \delta e^{-x^2} e^{-2ix\sqrt{\tau}H} + \mathcal{O}(\delta^2), \quad (40)$$

such that in the limit $\delta \rightarrow 0$ we recover the celebrated *Hubbard-Stratonovich* (HS) transformation [68–71]:

$$e^{-\tau H^2} = \frac{1}{\sqrt{\pi}} \int_{-\infty}^{\infty} e^{-x^2} e^{-2ix\sqrt{\tau}H} dx. \quad (41)$$

This result is usually understood as a correspondence linking a deterministic quadratic potential to a stochastic linear one. Here, however, it emerges in a generative manner from ITQDE as the continuous limit of infinitesimal dynamics where the state space and its dual are oppositely evolved. Based on this limit, it is in fact possible to infer a generalisation of the HS transformation by repeating the same limiting procedure, but beginning from a general initial state. Setting $|\psi_0\rangle = \sum_j a_j |E_j\rangle$, we find

$$\begin{aligned} & e^{-\tau(E_k+E_l)^2/4} |E_k\rangle \langle E_l| \\ &= \frac{1}{2^n} \sum_{j=-\frac{n}{2}}^{\frac{n}{2}} \binom{n}{\frac{n}{2}+j} e^{-2ij\sqrt{2d\tau}(E_k+E_l)} |E_k\rangle \langle E_l|. \end{aligned} \quad (42)$$

If we define the operator

$$\rho_{\text{mix}} = \sum_{kl} a_k a_l e^{-\tau(E_k E_l)/2} |E_k\rangle \langle E_l|, \quad (43)$$

then the previous $\delta \rightarrow 0$ limit then yields

$$\begin{aligned} & e^{-\tau H^2/2} \rho_{\text{mix}} e^{-\tau H^2/2} \\ &= \frac{1}{\sqrt{\pi}} \int_{-\infty}^{\infty} e^{-x^2} e^{-ix\sqrt{\tau}H} |\psi_0\rangle \langle \psi_0| e^{-ix\sqrt{\tau}H} dx. \end{aligned} \quad (44)$$

V. NUMERICAL ILLUSTRATIONS

To demonstrate the capability of Eq. (30) to resolve the spectrum of H , we now illustrate an application of this procedure to the 1D transverse field Ising model, which is a simple model composed of nearest-neighbor coupled spins on a lattice in the presence of an external, uniform magnetic field. It has been studied extensively over the years in the contexts of quantum phase transitions [72, 73], quantum spin glasses [74, 75], and the quantum annealing process [76–79] among others. It is also a useful benchmark problem for developing and testing quantum algorithms, as the model is exactly solvable [72, 80], and spins map naturally to qubits. The Hamiltonian is given by

$$H_{\text{TFIM}} = -J \sum_{l=0}^{L-1} Z_l Z_{l+1} - h \sum_{l=0}^{L-1} X_l, \quad (45)$$

where Z_l and X_l denote Pauli- Z and Pauli- X matrices, respectively, that act on the spin occupying lattice site l , J characterizes the strength of the nearest-neighbor interactions, h is the magnetic field strength, and L is the total number of lattice sites. Here, we consider a model

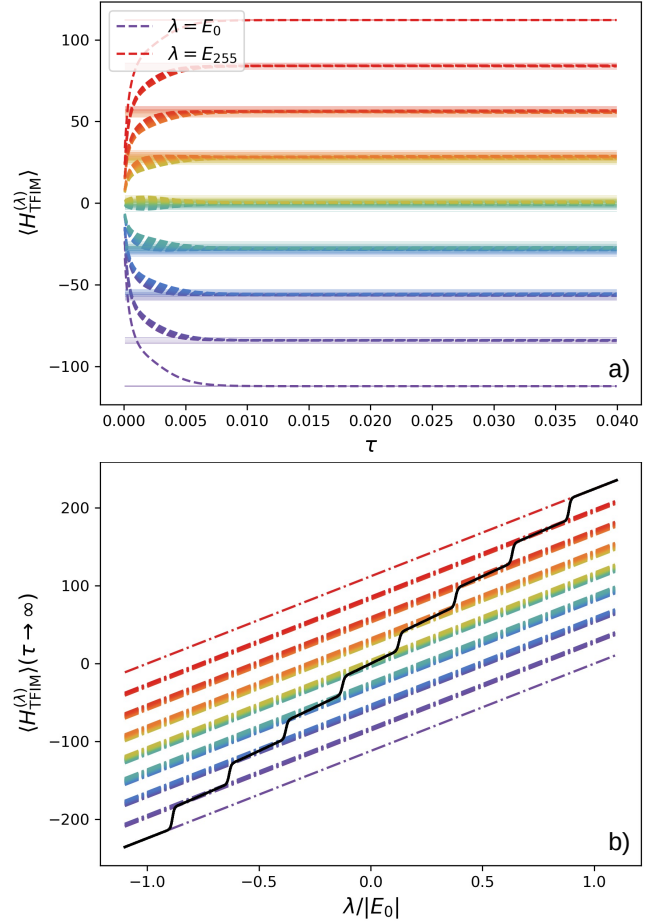


FIG. 2. Results of spectral calculations performed for an eight site Ising Hamiltonian using $\Delta\tau = 0.4 \times 10^{-5}$ and $m = 1000$. Dashed lines indicate the eigenenergies of H_{TFIM} . Solid lines indicate the convergence of the spectral calculation to these eigenenergies. For a), we plot the calculated energy as λ against propagation in imaginary time τ and find that our method converges to successively lower eigenstates of H_{TFIM} before reaching the ground state E_0 . For b), we plot the change in the steady state expectation value of H_{TFIM} as λ is varied, illustrating that a complete course-grained spectrum is obtainable using only expectation values estimated from a single trajectory only.

with $J = 1$, $h = 2$, $L = 8$, and open boundary conditions. We use Eqs. (30) and (31) to calculate the expectation value $\langle H_{\text{TFIM}}^{(\lambda)}(\tau) \rangle$ for different values of λ , which are plotted as a function of τ in Fig. 2(a). These results show that changing the value of λ causes $\langle H_{\text{TFIM}}^{(\lambda)}(\tau) \rangle$ to converge to different energies, corresponding in this case to the energies associated with each of the different bands of eigenstates. This premise is further reinforced in Fig. 2(b), where we plot the steady state expectation value $\langle H_{\text{TFIM}}^{(\lambda)}(\tau \rightarrow \infty) \rangle = \langle H_{\text{TFIM}}(\tau \rightarrow \infty) \rangle + \lambda$ against λ , from which the complete spectrum is inferred.

We demonstrate the use of the large m approximation by comparing the results obtained using Eqs. (32) and

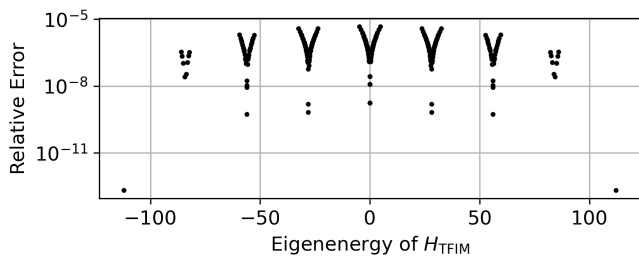


FIG. 3. Relative error calculated according to Eq. (46) in spectral calculations performed using the large m approximation in Eqs. (32) and (33) compared to the results obtained using Eqs. (30) and (31) for the 8 site 1D transverse field Ising model. In both cases, $\Delta\tau = 0.4 \times 10^{-5}$ and $m = 1000$

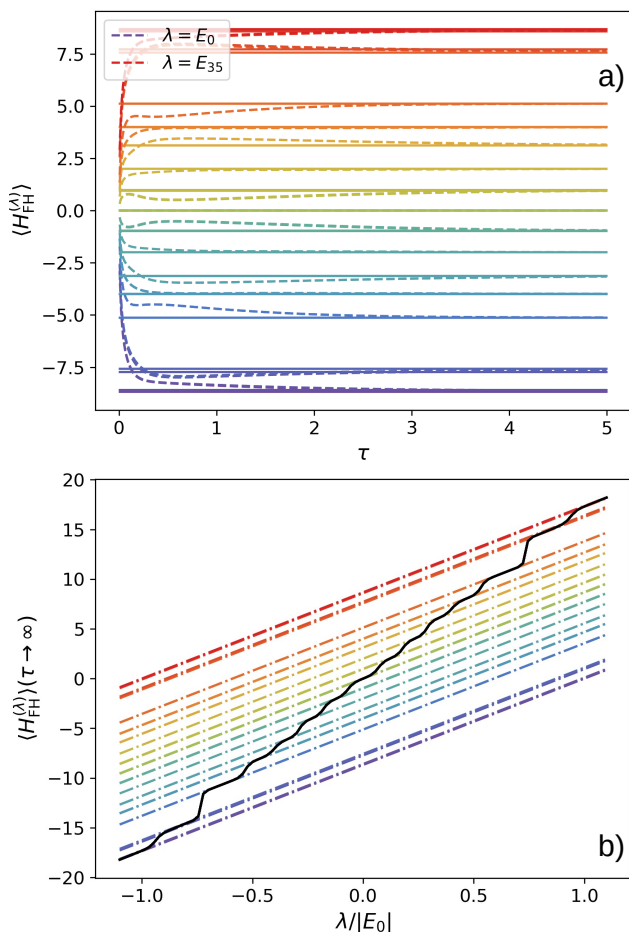


FIG. 4. Results of spectral calculations performed for a four site, 2D Fermi-Hubbard model at half-filling with $d\tau = 0.003$ and $m = 1500$. Dashed lines indicate the eigenenergies of H_{FH} , and solid lines show the convergence of $\langle H_{\text{FH}}^{(\lambda)} \rangle(\tau)$ to these eigenenergies. For a), we plot the calculated energy for various λ against τ , and observe good convergence to successively lower eigenstates of H_{FH} before reaching the ground state, E_0 . For b), we plot the change in the steady state expectation value, i.e., $\langle H_{\text{FH}}^{(\lambda)} \rangle(\tau \rightarrow \infty)$ as λ is varied, illustrating that a coarse-grained spectrum can be obtained.

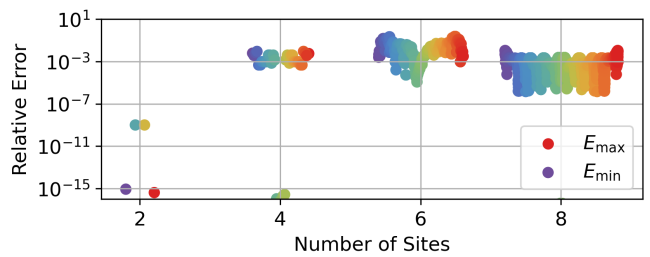


FIG. 5. Relative error in spectral calculations of the steady state expectation values for the eigenenergies of the 2D Fermi-Hubbard model at half-filling for 2, 4, 6, and 8 sites. Each eigenenergy error is plotted symmetrically about the spectral centre, which is aligned on the figure with the number of sites that spectrum corresponds to. All calculations were performed using a step size of $\Delta\tau = 0.003$ for $m = 1500$ steps to a final imaginary time $\tau = 5$ with the initial condition $\rho_{\text{FD}}(0) = I$.

(33) to the ones obtained using Eqs. (30) and (31) for this 8 site transverse field Ising model. The relative difference

$$\zeta = \frac{|\langle O^{(\lambda)} \rangle - \langle \tilde{O}^{(\lambda)} \rangle|}{|\langle O_g \rangle|}, \quad (46)$$

for each eigenenergy of H_{TFIM} is shown in Fig. 3. Here we use $\langle O_g \rangle$ as the minimum eigenenergy of H_{TFIM} to avoid dividing by small numbers when the calculated eigenvalue is near 0. This demonstrates that the large m approximation obtains results that are similar to the direct approach using the binomial coefficients.

We also apply the large m approximation to the 2D Fermi-Hubbard model. The Fermi-Hubbard model is a simple lattice model that aims to capture key aspects of strongly correlated fermionic systems, and has been used to study phase transitions [81], superconductivity [82], and magnetism [83]. The Hamiltonian is given by

$$H_{\text{FH}} = \sum_{\langle i,j \rangle, \sigma} t_{ij} (c_{i\sigma}^\dagger c_{j\sigma} + \text{h.c.}) + U \sum_{j=0}^{L-1} n_{j\uparrow} n_{j\downarrow} - \mu \sum_{j=0}^{L-1} n_{j\sigma}, \quad (47)$$

where t_{ij} denotes the tunneling amplitude between lattice sites i and j , $c_{j\sigma}^\dagger$ and $c_{j\sigma}$ are the creation and annihilation operators associated with a fermion of spin σ at lattice site j , respectively, U characterizes the on-site interaction of fermions, $n_{j\sigma} = c_{j\sigma}^\dagger c_{j\sigma}$ is the occupation number operator, μ is the chemical potential, and L is the number of lattice sites.

In Fig. 4(a), we plot results showing how the expectation value $\langle H_{\text{FH}}^{(\lambda)} \rangle(\tau)$ varies with τ and λ when the model parameters are set according to $t_{ij} = t = -1$ for all nearest-neighbor pairs, $U = 2$, $\mu = 0.5$, $L = 4$ (corresponding to a 2×2 lattice), and periodic boundary conditions. These results again demonstrate that changing λ causes $\langle H_{\text{FH}}^{(\lambda)} \rangle(\tau)$ to converge to different energies in the spectrum of H_{FH} and that reasonable results are obtained even when using the large m approximation. The

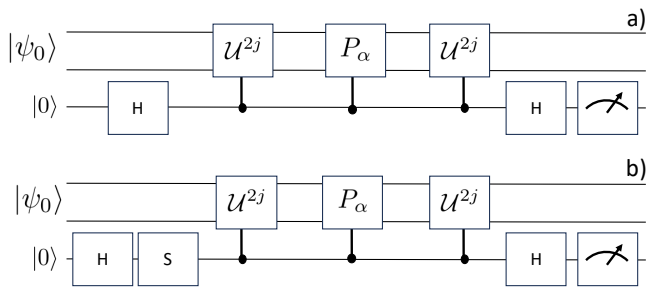


FIG. 6. Quantum circuits for performing Hadamard tests to estimate a) $\text{Re}(\langle\psi_{-2j}|P_\alpha|\psi_{2j}\rangle)$ and b) $\text{Im}(\langle\psi_{-2j}|P_\alpha|\psi_{2j}\rangle)$ for use in Eqs. (32) and (33). We denote by P_α the α -th Pauli string in the decomposition of the observable O , per Eq. (51). $H = \frac{1}{\sqrt{2}}\begin{pmatrix} 1 & 1 \\ 1 & -1 \end{pmatrix}$ and $S = \begin{pmatrix} 1 & 0 \\ 0 & i \end{pmatrix}$ denote the Hadamard and phase gate, respectively.

steady state expectation value $\langle H_{\text{FM}}^{(\lambda)} \rangle (\tau \rightarrow \infty)$ of this model for varying λ is plotted in Fig. 4(b) and further demonstrates that changing λ can be used to infer the energetic spectrum.

To examine the performance of our method as the number of sites in the 2D Fermi-Hubbard model increases, we calculate the relative error in the calculation of each eigenenergy compared to the exact values obtained by diagonalizing H_{FM} . This is plotted against the number of sites in the lattice in Fig. 5. We observe from these results that our method is able to accurately calculate the energy eigenvalues of the 2D Fermi-Hubbard model up to 8 sites and that the accuracy is not dependent on the number of sites in the lattice. The exception is the 2 site case, where much more accurate results are obtained. This is most likely due to the fact that in the case of 2 sites the model is effectively its much simpler one dimensional equivalent.

All of the results discussed in this section were obtained using the initial condition $\rho(0) = I$. In App. B, we discuss the effects of choosing a single pure state as the initial condition on the spectral calculation results.

VI. QUANTUM ALGORITHM FOR SPECTRAL CALCULATIONS USING ITQDE

We now present a proof-of-concept application of ITQDE to quantum computation. In particular, we implement ITQDE as a quantum algorithm, where a quantum computer is utilized to estimate the overlaps (i.e., of the form $\langle\psi_{-2j}|\psi_{2j}\rangle$ and $\langle\psi_{-2j}|O|\psi_{2j}\rangle$) that appear in Eqs. (30)-(33). We focus this section on how to construct a quantum algorithm for evaluating Eqs. (30)-(33) that is independent of the initial state $|\psi_0\rangle$, since in practice, $|\psi_0\rangle$ can be selected in a problem-dependent manner.

There are a number of methods by which the relevant overlaps might be calculated in a quantum computer (see for example App. D), but here we consider the most conceptually direct route provided by the Hadamard test

[84]. This requires only a single ancilla qubit, and is detailed fully in App. C. The Hadamard test functions by initializing the ancilla qubit in the state $|0\rangle$ and the primary system register in a state $|\varphi\rangle$, followed by Hadamard gates on the ancilla qubit, interleaved with a unitary operation \mathcal{W} that is applied to the primary system register and controlled on the state of the ancilla qubit, and culminating with a final ancilla qubit measurement [see Fig. 6(a)]. Repeating this procedure many times and averaging the results of the final ancilla measurement then outputs an estimate for the real part of the overlap between $|\varphi\rangle$ and $\mathcal{W}|\varphi\rangle$ in terms of the probability of measuring 0, p_0 on the ancilla qubit, such that

$$\text{Re}(\langle\varphi|\mathcal{W}|\varphi\rangle) = 2p_0 - 1. \quad (48)$$

A modified version of the Hadamard test, i.e., one that incorporates an additional phase gate on the ancilla qubit, can be used to obtain the imaginary part of the overlap in an analogous manner [see Fig. 6(b)].

In order to utilize the Hadamard test in our setting, we now discuss approaches for using it to estimate $\langle\psi_{-2j}|\psi_{2j}\rangle$ and $\langle\psi_{-2j}|O|\psi_{2j}\rangle$, beginning with the former, which can be expressed as

$$\langle\psi_{-2j}|\psi_{2j}\rangle = \langle\psi_0|\mathcal{U}^{4j}|\psi_0\rangle. \quad (49)$$

Hadamard tests can be performed to estimate the real and imaginary parts of the right-hand-side of Eq. (49) by associating $\mathcal{W} = \mathcal{U}^{4j} = e^{-i\sqrt{2j}\Delta\tau H}$ and $|\varphi\rangle = |\psi_0\rangle$ in Eq. (48).

In order to estimate overlaps of the second form, $\langle\psi_{-2j}|O|\psi_{2j}\rangle$, we first expand O in the Pauli operator basis according to

$$O = \sum_{\alpha=1}^M c_\alpha P_\alpha, \quad (50)$$

where c_α and P_α denote a real coefficient and Pauli basis operator, respectively. We assume that $M = \text{poly}(n)$, noting that when O is taken to be a k -local observable, this assumption holds. Importantly, because the Pauli operators are unitary, this expansion allows us to then estimate $\langle\psi_{-2j}|O|\psi_{2j}\rangle$ by taking the sum of a linear combination of constituent overlaps, each evaluated using separate Hadamard tests, according to

$$\langle\psi_{-2j}|O|\psi_{2j}\rangle = \sum_{\alpha=1}^M c_\alpha \langle\psi_0|\mathcal{U}^{2j} P_\alpha \mathcal{U}^{2j}|\psi_0\rangle, \quad (51)$$

where for the α -th Hadamard test, we have $\mathcal{W} = \mathcal{U}^{2j} P_\alpha \mathcal{U}^{2j}$, and M Hadamard tests are needed in total to evaluate Eq. (51). Using this approach to estimate the real and imaginary parts of all $\frac{m}{2} + 1$ overlaps in Eqs. (32) and (33) then requires $(m+2)(M+1) = \mathcal{O}(mM)$ separate circuits (each repeated sufficiently many times to ensure convergence of the estimate).

Given this Hadamard test formulation, a method for implementing the (real) time evolution $\mathcal{U}^{4j} = e^{-i\sqrt{2j}\Delta\tau H}$

on the primary system register is then all that is additionally required to complete the specification of the quantum algorithm. It is worth noting that in order to simulate imaginary time evolution by an imaginary time τ under a Hamiltonian H^2 , we only need real time evolution under H by time $\sqrt{2\Delta\tau}$. For physically-realistic Hamiltonians, it is known that U^{4j} can be implemented *efficiently* on a quantum computer [85] via a variety of different Hamiltonian simulation algorithms that proceed in a time that scales as $\text{poly}(n)$ on n qubits.

Quantum device implementations

Finally, we present the results from implementing ITQDE directly on quantum devices. For this, we utilize the IBM superconducting qubit processor `ibm_brisbane`, along with IBM's sampler primitive [86]. Our first implementation considers the transverse field Ising model with $J = 1$, $h = 2$, $L = 2$, and the results are presented in Fig. 7. In this demonstration, the quantum dynamical emulation procedure is repeated for 104 different initial states, prepared by applying random Clifford operations to the initial $|00\rangle$ state, and averaging the overlaps at each step. This averaging procedure (over initial Clifford realizations) aims to produce statistics that converge, with increasing realizations, to those that would be obtained with an initialization in the maximally mixed state. We expect that the convergence towards the middle energies could be improved by sampling initial states from additional random Cliffords.

VII. OUTLOOK

In this work we have proposed a method for constructing the solutions of non-unitary dynamics from purely unitary operations, which we term Quantum Dynamical Emulation. This was applied in the context of imaginary time to derive the ITQDE correspondence between real and imaginary time evolution. This in effect provides a unitary representation of a non-unitary evolution, which has been exploited here to develop a quantum algorithm for spectral calculations. The results presented here represent a first application of quantum dynamical emulation; however, this technique is ripe for further refinement in terms of approximations to improve its efficiency, in the scope of its application, and in understanding its limitations. ITQDE is after all an approximate equivalence based on a discretisation, and it is clear that the success of this approximation will depend upon the interplay of free parameters such as $\Delta\tau$ and λ , as well as the type of Hamiltonian being studied. There is after all no such thing as a free lunch, and a likely approach to refining this technique will be understanding where the computational complexity implied by the ability to calculate spectra lies.

For example, the error in the present approximation

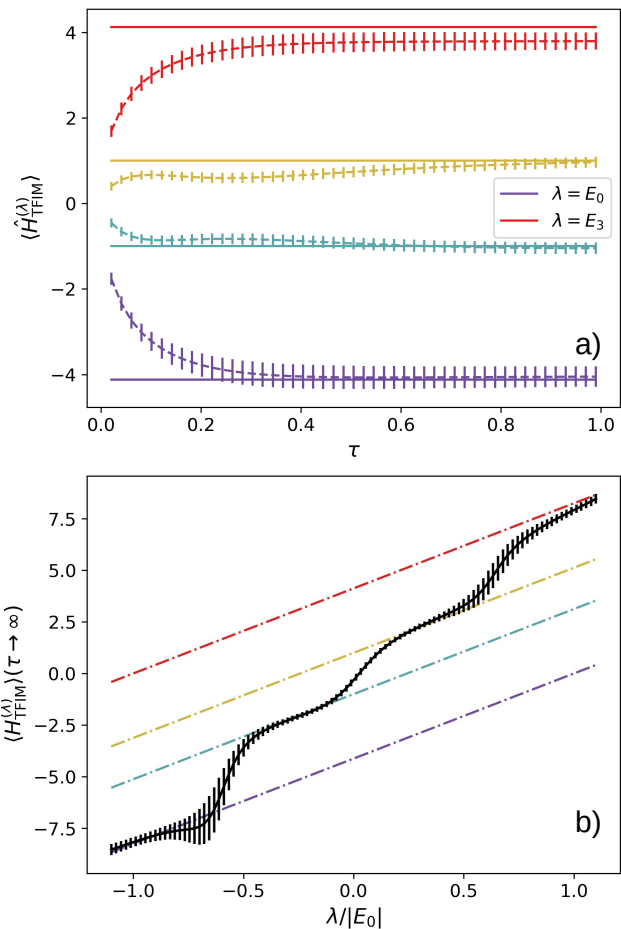


FIG. 7. Spectral calculation results for a 2-site transverse field Ising model with $J = 1$ and $h = 2$, obtained via implementation of ITQDE on an IBM superconducting qubit processor (`ibm_brisbane`). Here we use $\Delta\tau = 0.01$ and $m = 100$. In a), the expectation values $\langle H_{TFIM}^{(\lambda)} \rangle(\tau)$ output from Eqs. (32) and (33), with overlaps obtained from `ibm_brisbane`, are shown (dashed curves) against the true eigenenergies (solid lines of corresponding color). Each overlap is obtained using 4000 samples. In b), the change in the steady state expectation of H_{TFIM} as λ changes is shown, illustrating that the coarse-grained spectrum can still be inferred when performing ITQDE on quantum hardware. In both figures, the errorbars denote 95% confidence.

is of order $\Delta\tau$, and while in the cases considered thus far this has not proved problematic, an immediate avenue for future investigation will be how to improve upon the order of this error. This could be achieved either by the application of RK4-like techniques, or from instead working backwards from the continuous limit of the H-S transform. In such a case, the use of techniques such as Gaussian quadrature may be employed to obtain highly accurate discretisations while requiring relatively few points. This procedure is sketched in App. E, together with an error bound for such an approach. This would not only have the potential to improve accuracy, but do so while reducing the required number of overlaps

for effective implementation of ITQDE.

While the majority of the calculations presented in this work use the large m approximations in Eqs. (32) and (33) to avoid calculating very large factorials, the exponential weighting means that most of the weight in the calculation is focused around the initial state and short-time overlaps. Embracing this feature may allow for truncated expressions with the potential to extrapolate out to much later τ than would otherwise be possible. This would allow for calculations with much shallower circuit depths than direct implementation would require.

As a proof-of-concept, ITQDE has been successfully applied to the calculation of spectral calculations on current quantum hardware. Prioritising conceptual clarity over performance, this has been achieved via the Hadamard test methodology for overlap measurement. This method’s use of controlled unitaries however means that it is a technique best suited to fault-tolerant computation. At present however quantum computing remains a NISQy business, and for this reason interferometric protocols that forego such controlled operations [87–89] are likely to be more suitable for the implementation of ITQDE in present hardware. An immediate application of such an approach would be in order to perform topological data analysis using recently proposed imaginary time methods [90].

Beyond the near term, the asymptotic scaling of ITQDE when combined with post-Trotter methods of implementation remains to be investigated. For example, while in a naive Trotterisation of the propagator, the circuit depth will scale with time, techniques such as Cartan decomposition [91] fix this depth for all times. Furthermore proposals for the estimation of thermal states [60] employ techniques such as block encodings based on Linear Combination of Unitaries and the TTS algorithm [92], and these same techniques may also be applied to future implementations of ITQDE. Given ITQDE’s ready adaptability to both fault-tolerant and NISQ friendly methods of implementation, it is likely to find application both in the present, and in a future where large-scale, fault tolerant quantum computers become a reality. In fact, we expect the question of efficient implementation in both the near and far term - together with a comparative study to existing methods for imaginary time and spectral calculations - to be addressed in forthcoming work.

More broadly, the fact that ITQDE reconstructs spectra using only measurement overlaps means the method is platform agnostic, and can be applied not only to a quantum circuit context, but any scenario in which such overlaps can be measured. A future research question is therefore whether ITQDE can be efficiently combined with other techniques (e.g. quantum state tomography), such that these overlaps are explicitly recoverable from measurements in as broad a context as possible. Moreover, as alluded to in Sec. V, the indirect manner in which H^2 is introduced into calculations potentially circumvents the issues which usually prevent the spectral

sweeps demonstrated here from being implemented in a Monte-Carlo setting. The fusion of these two approaches to imaginary time simulation could therefore constitute a further source of inspiration for extending ITQDE.

We have also provided a preliminary sketch of potential uses for ITQDE in the context of stochastic and quantum thermodynamics. Given these results, it is difficult to resist the impression of deep links between ITQDE and thermodynamic theory. We expect that continued study of these connections have the potential to yield both surprising and useful results. In fact, while the work performed here has restricted itself to a quantum setting, Hilbert space representations of classical dynamics [93–96] - including the recently developed waveoperator representation [97] - represent excellent prospects for applying both the current work and its future extensions to the domain of classical dynamics.

Finally, we reiterate that ITQDE is a proof of concept for the more general procedure of QDE. The objective of unitary representations of non-unitary dynamics has recently produced a number of proposals [98, 99], but while all these approaches are animated by the same motive, the methods used to achieve this stand in stark contrast. A natural question then for future work is to understand the commonalities in these approaches, perhaps with an eventual view towards their amalgamation. In the near term, the next implementation of QDE is likely a form of Lindbladian dynamics based on Ref.[50], which could in turn be applied to the realisation of recent proposals for error-mitigation in quantum simulation [100]. More fundamentally, an open question for QDE is both the limit of what exotic states might be expressible via an operator-valued differential equation, and the degree to which QDE renders them realisable and computable.

In closing this paper, we have attempted to highlight the many opportunities and challenges promised by the present work. It should be considered as an invitation to the broader physics community, with its diversity of interests and expertise, to seize this opportunity to attack questions old and new with a fresh perspective. We therefore close on a note we hope reflects the sense of adventure we have felt, and continue to feel in this ongoing work. With QDE, the imaginary has become reality.

ACKNOWLEDGMENTS

The authors would like to thank Alicia Magann and Christian Arenz for their vital contributions, without which the present work would have been impossible. J.M.L. is supported by Sandia National Laboratories’ Laboratory Directed Research and Development Program. G.M. and D.I.B. were supported by the Army Research Office (grant W911NF-23-1-0288; program manager Dr. James Joseph). Sandia National Laboratories is a multimission laboratory managed and operated by National Technology & Engineering Solutions of Sandia, LLC, a wholly owned subsidiary of Honeywell Interna-

tional Inc., for the U.S. Department of Energy's National Nuclear Security Administration under contract DE-NA0003525. This article has been authored by an employee of National Technology & Engineering Solutions of Sandia, LLC under Contract No. DE-NA0003525 with the U.S. Department of Energy (DOE). The employee owns all right, title and interest in and to the article and is solely responsible for its contents. The United States Government retains and the publisher, by accepting the article for publication, acknowledges that the United States Government retains a non-exclusive,

paid-up, irrevocable, world-wide license to publish or reproduce the published form of this article or allow others to do so, for United States Government purposes. The DOE will provide public access to these results of federally sponsored research in accordance with the DOE Public Access Plan <https://www.energy.gov/downloads/doe-public-access-plan>. This paper describes objective technical results and analysis. Any subjective views or opinions that might be expressed in the paper do not necessarily represent the views of the U.S. Department of Energy, Army Research Office, or the United States Government. SAND2024-02496O.

-
- [1] G. C. Wick, Properties of bethe-salpeter wave functions, *Phys. Rev.* **96**, 1124 (1954).
- [2] Y. Yang, H. Li, L. Sheng, R. Shen, D. N. Sheng, and D. Y. Xing, Topological phase transitions with and without energy gap closing, *New Journal of Physics* **15**, 083042 (2013), publisher: IOP Publishing.
- [3] M. B. Hastings and T. Koma, Spectral Gap and Exponential Decay of Correlations, *Communications in Mathematical Physics* **265**, 781 (2006).
- [4] T. S. Cubitt, D. Perez-Garcia, and M. M. Wolf, Undecidability of the spectral gap, *Nature* **528**, 207 (2015).
- [5] T.-H. Han, J. S. Helton, S. Chu, D. G. Nocera, J. A. Rodriguez-Rivera, C. Broholm, and Y. S. Lee, Fractionalized excitations in the spin-liquid state of a kagome-lattice antiferromagnet, *Nature* **492**, 406 (2012), number: 7429 Publisher: Nature Publishing Group.
- [6] L. Balents, Spin liquids in frustrated magnets, *Nature* **464**, 199 (2010), number: 7286 Publisher: Nature Publishing Group.
- [7] M. J. Hartmann, M. E. Reuter, and M. B. Plenio, Excitation and entanglement transfer versus spectral gap, *New Journal of Physics* **8**, 94 (2006).
- [8] D. Jacquemin, B. Mennucci, and C. Adamo, Excited-state calculations with TD-DFT: from benchmarks to simulations in complex environments, *Physical Chemistry Chemical Physics* **13**, 16987 (2011), publisher: Royal Society of Chemistry.
- [9] P. Ramos and M. Pavanello, Low-lying excited states by constrained DFT, *The Journal of Chemical Physics* **148**, 144103 (2018), publisher: American Institute of Physics.
- [10] N. Ferré, M. Filatov, and M. Huix-Rotllant, eds., *Density-Functional Methods for Excited States*, Topics in Current Chemistry, Vol. 368 (Springer International Publishing, Cham, 2016).
- [11] U. Kaldor, Degenerate many-body perturbation theory: Excited states of H_2 , *The Journal of Chemical Physics* **63**, 2199 (1975).
- [12] M. S. Hybertsen and S. G. Louie, Electron correlation in semiconductors and insulators: Band gaps and quasiparticle energies, *Physical Review B* **34**, 5390 (1986), publisher: American Physical Society.
- [13] M. S. Hybertsen and S. G. Louie, First-Principles Theory of Quasiparticles: Calculation of Band Gaps in Semiconductors and Insulators, *Physical Review Letters* **55**, 1418 (1985), publisher: American Physical Society.
- [14] R. W. Godby, M. Schlüter, and L. J. Sham, Accurate Exchange-Correlation Potential for Silicon and Its Discontinuity on Addition of an Electron, *Physical Review Letters* **56**, 2415 (1986), publisher: American Physical Society.
- [15] R. W. Godby, M. Schlüter, and L. J. Sham, Self-energy operators and exchange-correlation potentials in semiconductors, *Physical Review B* **37**, 10159 (1988), publisher: American Physical Society.
- [16] R. J. Hunt, M. Szyniszewski, G. I. Prayogo, R. Maezono, and N. D. Drummond, Quantum Monte Carlo calculations of energy gaps from first principles, *Physical Review B* **98**, 075122 (2018).
- [17] D. Blume, M. Lewerenz, P. Niyaz, and K. B. Whaley, Excited states by quantum Monte Carlo methods: Imaginary time evolution with projection operators, *Physical Review E* **55**, 3664 (1997), publisher: American Physical Society.
- [18] A. Lüchow, D. Neuhauser, J. Ka, R. Baer, J. Chen, and V. A. Mandelshtam, Computing Energy Levels by Inversion of Imaginary-Time Cross-Correlation Functions, *The Journal of Physical Chemistry A* **107**, 7175 (2003).
- [19] C.-C. Chou and D. J. Kouri, Multidimensional Supersymmetric Quantum Mechanics: A Scalar Hamiltonian Approach to Excited States by the Imaginary Time Propagation Method, *The Journal of Physical Chemistry A* **117**, 3449 (2013), publisher: American Chemical Society.
- [20] L. K. Joshi, A. Elben, A. Vikram, B. Vermersch, V. Galitski, and P. Zoller, Probing Many-Body Quantum Chaos with Quantum Simulators, *Phys. Rev. X* **12**, 011018 (2022), publisher: American Physical Society.
- [21] P. J. J. Luukko and E. Räsänen, Imaginary time propagation code for large-scale two-dimensional eigenvalue problems in magnetic fields, *Computer Physics Communications* **184**, 769 (2013).
- [22] R. J. Needs, M. D. Towler, N. D. Drummond, and P. López Ríos, Continuum variational and diffusion quantum Monte Carlo calculations, *Journal of Physics: Condensed Matter* **22**, 023201 (2010).
- [23] L. Lehtovaara, J. Toivanen, and J. Eloranta, Solution of time-independent Schrödinger equation by the imaginary time propagation method, *Journal of Computational Physics* **221**, 148 (2007).
- [24] S. A. Chin, S. Janecek, and E. Krotscheck, Any order imaginary time propagation method for solving the

- Schrödinger equation, *Chemical Physics Letters* **470**, 342 (2009).
- [25] H. Tasaki, The Hubbard model - An introduction and selected rigorous results, *J. Phys. Cond. Mat.* **10**, 4353 (1998).
- [26] W. Ren, W. Fu, X. Wu, and J. Chen, Towards the ground state of molecules via diffusion Monte Carlo on neural networks, *Nature Communications* **14**, 10.1038/s41467-023-37609-3 (2023), number: 1 Publisher: Nature Publishing Group.
- [27] A. M. Köster, P. Calaminici, E. Orgaz, D. R. Roy, J. U. Reveles, and S. N. Khanna, On the Ground State of Pd13, *Journal of the American Chemical Society* **133**, 12192 (2011), publisher: American Chemical Society.
- [28] D. M. Ceperley and B. J. Alder, Ground State of the Electron Gas by a Stochastic Method, *Physical Review Letters* **45**, 566 (1980), publisher: American Physical Society.
- [29] J. Chen and E. M. Stoudenmire, Hybrid purification and sampling approach for thermal quantum systems, *Physical Review B* **101**, 195119 (2020), publisher: American Physical Society.
- [30] A. Sinha, M. M. Rams, and J. Dziarmaga, Efficient representation of minimally entangled typical thermal states in two dimensions via projected entangled pair states, *Physical Review B* **109**, 045136 (2024), publisher: American Physical Society.
- [31] W. Kadow, F. Pollmann, and M. Knap, Isometric tensor network representations of two-dimensional thermal states, *Physical Review B* **107**, 205106 (2023), publisher: American Physical Society.
- [32] C. Gogolin, M. P. Müller, and J. Eisert, Absence of thermalization in nonintegrable systems, *Phys. Rev. Lett.* **106**, 040401 (2011).
- [33] C. Gogolin and J. Eisert, Equilibration, thermalisation, and the emergence of statistical mechanics in closed quantum systems, *Reports on Progress in Physics* **79**, 056001 (2016).
- [34] M. Cramer, Thermalization under randomized local hamiltonians, *New Journal of Physics* **14**, 053051 (2012).
- [35] I. Reichental, A. Klempner, Y. Kafri, and D. Podolsky, Thermalization in open quantum systems, *Phys. Rev. B* **97**, 134301 (2018).
- [36] T. Shirai, T. Mori, and S. Miyashita, Floquet–Gibbs state in open quantum systems, *Eur. Phys. J. Spec. Top.* **227**, 323 (2018).
- [37] S. Kirkpatrick, C. D. Gelatt, and M. P. Vecchi, Optimization by simulated annealing, *Science* **220**, 671 (1983), <https://www.science.org/doi/pdf/10.1126/science.220.4598.671>.
- [38] F. Krzakala, A. Montanari, F. Ricci-Tersenghi, G. Semerjian, and L. Zdeborova, Gibbs states and the set of solutions of random constraint satisfaction problems, *Proceedings of the National Academy of Sciences* **104**, 10318 (2007), <https://www.pnas.org/doi/pdf/10.1073/pnas.0703685104>.
- [39] G. H. Low and I. L. Chuang, Optimal hamiltonian simulation by quantum signal processing, *Phys. Rev. Lett.* **118**, 010501 (2017).
- [40] Z. Jiang, K. J. Sung, K. Kechedzhi, V. N. Smelyanskiy, and S. Boixo, Quantum algorithms to simulate many-body physics of correlated fermions, *Physical Review Applied* **9**, 044036 (2018).
- [41] L. Wright, F. Barratt, J. Dborin, G. H. Booth, and A. G. Green, Automatic post-selection by ancillae thermalization, *Phys. Rev. Res.* **3**, 033151 (2021).
- [42] F. Turro, A. Roggero, V. Amitrano, P. Luchi, K. A. Wendt, J. L. Dubois, S. Quaglioni, and F. Pederiva, Imaginary-time propagation on a quantum chip, *Physical Review A* **105**, 022440 (2022).
- [43] S. McArdle, S. Endo, A. Aspuru-Guzik, S. C. Benjamin, and X. Yuan, Quantum computational chemistry, *Rev. Mod. Phys.* **92**, 015003 (2020).
- [44] M. Kondappan, M. Chaudhary, E. O. Ilo-Okeke, V. Ivannikov, and T. Byrnes, Imaginary-time evolution with quantum nondemolition measurements: Multi-qubit interactions via measurement nonlinearities, *Phys. Rev. A* **107**, 042616 (2023), publisher: American Physical Society.
- [45] T. Kosugi, H. Nishi, and Y.-i. Matsushita, Exhaustive search for optimal molecular geometries using imaginary-time evolution on a quantum computer, *npj Quantum Inf* **9**, 1 (2023), number: 1 Publisher: Nature Publishing Group.
- [46] P. Jouzdani, C. W. Johnson, E. R. Mucciolo, and I. Stetcu, Alternative approach to quantum imaginary time evolution, *Phys. Rev. A* **106**, 062435 (2022).
- [47] K. Hejazi, M. Motta, and G. K.-L. Chan, Adiabatic quantum imaginary time evolution (2023), arXiv:2308.03292 [quant-ph].
- [48] M. Motta, C. Sun, A. T. K. Tan, M. J. O’Rourke, E. Ye, A. J. Minnich, F. G. S. L. Brandão, and G. K.-L. Chan, Determining eigenstates and thermal states on a quantum computer using quantum imaginary time evolution, *Nature Physics* **16**, 205 (2020).
- [49] T. Kosugi, Y. Nishiya, H. Nishi, and Y.-i. Matsushita, Imaginary-time evolution using forward and backward real-time evolution with a single ancilla: First-quantized eigensolver algorithm for quantum chemistry, *Phys. Rev. Res.* **4**, 033121 (2022).
- [50] G. McCaul, K. Jacobs, and D. I. Bondar, Fast computation of dissipative quantum systems with ensemble rank truncation, *Phys. Rev. Research* **3**, 013017 (2021).
- [51] C. Le Bris and P. Rouchon, Low-rank numerical approximations for high-dimensional Lindblad equations, *Phys. Rev. A* **87**, 022125 (2013).
- [52] S. Finazzi, A. Le Boité, F. Storme, A. Baksic, and C. Ciuti, Corner-Space Renormalization Method for Driven-Dissipative Two-Dimensional Correlated Systems, *Phys. Rev. Lett.* **115**, 080604 (2015).
- [53] K. Donatella, Z. Denis, A. Le Boité, and C. Ciuti, Continuous-time dynamics and error scaling of noisy highly entangling quantum circuits, *Phys. Rev. A* **104**, 062407 (2021).
- [54] J. Spencer, *Asymptopia*, Student mathematical library (American Mathematical Society, Providence, RI, 2014).
- [55] J. M. Leamer, W. Dawson, and D. I. Bondar, Positivity preserving density matrix minimization at finite temperatures via square root (2023), arXiv:2103.07078.
- [56] D. I. Bondar, A. G. Campos, R. Cabrera, and H. A. Rabitz, Efficient computations of quantum canonical Gibbs state in phase space, *Physical Review E* **93**, 10.1103/PhysRevE.93.063304 (2016).
- [57] J. E. Hirsch and J. R. Schrieffer, Dynamic correlation functions in quantum systems: A Monte Carlo algorithm, *Physical Review B* **28**, 5353 (1983), publisher:

- American Physical Society.
- [58] J. E. Hirsch and J. R. Schrieffer, Dynamic correlation functions in quantum systems: A monte carlo algorithm, *Phys. Rev. B* **28**, 5353 (1983).
- [59] D. M. Ceperley and B. Bernu, The calculation of excited state properties with quantum monte carlo, *The Journal of Chemical Physics* **89**, 6316–6328 (1988).
- [60] A. N. Chowdhury and R. D. Somma, *Quantum algorithms for Gibbs sampling and hitting-time estimation* (2016), arXiv:1603.02940 [quant-ph].
- [61] G. McCaul and D. I. Bondar, How to win friends and influence functionals: deducing stochasticity from deterministic dynamics, *The European Physical Journal Special Topics* **230**, 733 (2021).
- [62] U. Seifert, Stochastic thermodynamics, fluctuation theorems and molecular machines, *Repo. Prog. Phys.* **75**, 126001 (2012).
- [63] R. E. Spinney and I. J. Ford, *Fluctuation relations: a pedagogical overview* (2012) pp. 1–58, arXiv:1201.6381.
- [64] G. E. Crooks, Entropy production fluctuation theorem and the nonequilibrium work relation for free energy differences, *Phys. Rev. E* **60**, 2721 (1999).
- [65] R. Kubo, The fluctuation-dissipation theorem, *Reports on Progress in Physics* **29**, 255 (1966).
- [66] S. H. Shenker and D. Stanford, Black holes and the butterfly effect, *Journal of High Energy Physics* **2014**, 10.1007/jhep03(2014)067 (2014).
- [67] A. Touil and S. Deffner, Information scrambling – a quantum thermodynamic perspective (2024), arXiv:2401.05305.
- [68] J. Hubbard, Calculation of partition functions, *Phys. Rev. Lett.* **3**, 77 (1959).
- [69] G. M. G. McCaul, C. D. Lorenz, and L. Kantorovich, Partition-free approach to open quantum systems in harmonic environments: An exact stochastic liouville equation, *PRB* **95**, 125124 (2017).
- [70] G. M. G. McCaul, C. D. Lorenz, and L. Kantorovich, Driving spin-boson models from equilibrium using exact quantum dynamics, *PRB* **97**, 224310 (2018).
- [71] G. McCaul and D. I. Bondar, How to win friends and influence functionals: deducing stochasticity from deterministic dynamics, *EPJST* **230**, 733 (2021).
- [72] J. Dziarmaga, Dynamics of a Quantum Phase Transition: Exact Solution of the Quantum Ising Model, *Physical Review Letters* **95**, 245701 (2005).
- [73] S. Sachdev, *Quantum phase transitions* (Cambridge University Press, Cambridge ; New York, 1999).
- [74] T. K. Kopeć, K. D. Usadel, and G. Büttner, Instabilities in the quantum Sherrington-Kirkpatrick Ising spin glass in transverse and longitudinal fields, *Physical Review B* **39**, 12418 (1989), publisher: American Physical Society.
- [75] C. Laumann, A. Scardicchio, and S. L. Sondhi, Cavity method for quantum spin glasses on the Bethe lattice, *Physical Review B* **78**, 134424 (2008), publisher: American Physical Society.
- [76] E. Farhi, J. Goldstone, S. Gutmann, and M. Sipser, *Quantum Computation by Adiabatic Evolution* (2000), arXiv:quant-ph/0001106.
- [77] T. F. Rønnow, Z. Wang, J. Job, S. Boixo, S. V. Isakov, D. Wecker, J. M. Martinis, D. A. Lidar, and M. Troyer, Defining and detecting quantum speedup, *Science* **345**, 420 (2014), <https://www.science.org/doi/pdf/10.1126/science.1252319>.
- [78] S. W. Shin, G. Smith, J. A. Smolin, and U. Vazirani, *How “Quantum” is the D-Wave Machine?* (2014), arXiv:1401.7087 [quant-ph].
- [79] S. Boixo, T. F. Rønnow, S. V. Isakov, Z. Wang, D. Wecker, D. A. Lidar, J. M. Martinis, and M. Troyer, Evidence for quantum annealing with more than one hundred qubits, *Nature Physics* **10**, 218 (2014), number: 3 Publisher: Nature Publishing Group.
- [80] P. Weinberg and M. Bukov, QuSpin: a Python package for dynamics and exact diagonalisation of quantum many body systems. Part II: bosons, fermions and higher spins, *SciPost Physics* **7**, 020 (2019).
- [81] M. Imada, A. Fujimori, and Y. Tokura, Metal-insulator transitions, *Rev. Mod. Phys.* **70**, 1039 (1998).
- [82] P. W. Anderson, The resonating valence bond state in La_2CuO_4 and superconductivity, *Science* **235**, 1196 (1987).
- [83] C. Hofrichter, L. Riegger, F. Scazza, M. Höfer, D. R. Fernandes, I. Bloch, and S. Fölling, Direct probing of the mott crossover in the $\text{SU}(n)$ fermi-hubbard model, *Phys. Rev. X* **6**, 021030 (2016).
- [84] R. Cleve, A. Ekert, C. Macchiavello, and M. Mosca, Quantum algorithms revisited, *Proceedings of the Royal Society of London. Series A: Mathematical, Physical and Engineering Sciences* **454**, 339 (1998).
- [85] S. Lloyd, Universal quantum simulators, *Science* **273**, 1073 (1996).
- [86] Qiskit contributors, *Qiskit: An open-source framework for quantum computing* (2021).
- [87] C. L. Cortes and S. K. Gray, Quantum krylov subspace algorithms for ground- and excited-state energy estimation, *Phys. Rev. A* **105**, 022417 (2022).
- [88] O. Kyriienko, Quantum inverse iteration algorithm for programmable quantum simulators, *npj Quantum Information* **6**, 10.1038/s41534-019-0239-7 (2020).
- [89] S. Scali, C. Umeano, and O. Kyriienko, Quantum topological data analysis via the estimation of the density of states (2023), arXiv:2312.07115.
- [90] S. Scali, C. Umeano, and O. Kyriienko, The topology of data hides in quantum thermal states (2024), arXiv:2402.15633.
- [91] N. Khaneja and S. J. Glaser, Cartan decomposition of $\text{su}(2n)$ and control of spin systems, *Chemical Physics* **267**, 11 (2001).
- [92] D. W. Berry, A. M. Childs, R. Cleve, R. Kothari, and R. D. Somma, Simulating hamiltonian dynamics with a truncated taylor series, *Phys. Rev. Lett.* **114**, 090502 (2015).
- [93] D. Chruściński, Koopman’s approach to dissipation, *Rep. Math. Phys.* **57**, 319 (2006).
- [94] G. McCaul, A. Pechen, and D. I. Bondar, Entropy non-conservation and boundary conditions for hamiltonian dynamical systems, *Phys. Rev. E* **99**, 062121 (2019).
- [95] G. McCaul and D. I. Bondar, Free to harmonic unitary transformations in quantum and Koopman dynamics*, *Journal of Physics A: Mathematical and Theoretical* **55**, 434003 (2022).
- [96] D. I. Bondar, R. Cabrera, D. V. Zhdanov, and H. A. Rabitz, Wigner phase-space distribution as a wave function, *Phys. Rev. A* **88**, 052108 (2013), arXiv:1202.3628.
- [97] G. McCaul, D. V. Zhdanov, and D. I. Bondar, Wave operator representation of quantum and classical dynamics, *Phys. Rev. A* **108**, 052208 (2023).
- [98] D. An, J.-P. Liu, and L. Lin, Linear combination of hamiltonian simulation for nonunitary dynamics with

optimal state preparation cost, *Phys. Rev. Lett.* **131**, 150603 (2023).

- [99] S. Jin, N. Liu, and Y. Yu, Quantum simulation of partial differential equations: Applications and detailed analysis, *Phys. Rev. A* **108**, 032603 (2023).
- [100] M. Rossini, D. Maile, J. Ankerhold, and B. I. C. Donvil, Single-qubit error mitigation by simulating non-markovian dynamics, *Phys. Rev. Lett.* **131**, 110603 (2023).
- [101] DLMF, *NIST Digital Library of Mathematical Functions*, <https://dlmf.nist.gov/>, Release 1.1.10 of 2023-06-15, f. W. J. Olver, A. B. Olde Daalhuis, D. W. Lozier, B. I. Schneider, R. F. Boisvert, C. W. Clark, B. R. Miller, B. V. Saunders, H. S. Cohl, and M. A. McClain, eds.

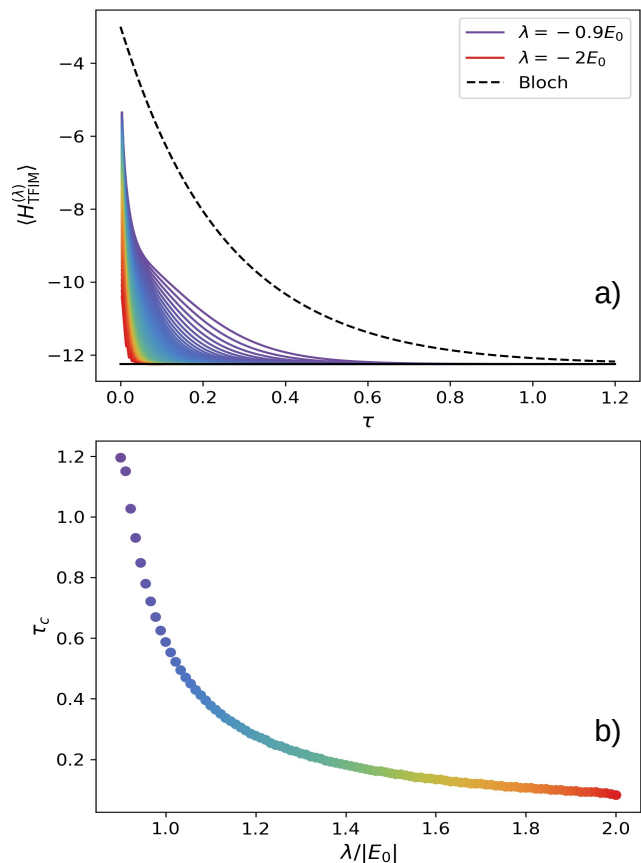


FIG. 8. Illustration of the convergence to the ground state in a transverse field Ising model. In all cases, convergence is achieved significantly faster than evolution with the Bloch equation. The bottom panel demonstrates how τ_c - the temperature at which $|\langle H \rangle - E_0| < 10^{-4}$ (E_0 being the ground state energy) - has the expected exponential dependence on λ .

Appendix A: Ground State Acceleration via λ

Here, we discuss how tuning λ can markedly improve the rate of convergence to the ground state with respect to τ . This phenomenon can be most easily illustrated with the case of a two level Hamiltonian. We denote the energies of the two levels in terms of the average energy \bar{E} and difference 2Δ , i.e. $E_0 = \bar{E} - \Delta$ and $E_1 = \bar{E} + \Delta$. If one were to evolve via the Bloch equation i.e.

$$\frac{d\rho}{d\tau} = -\frac{1}{2}\{\rho, H\} \quad (\text{A1})$$

one would obtain (after normalisation) the Gibbs state

$$\frac{1}{Z}e^{-\tau(H-\lambda)} = \frac{1}{Z}(e^{\tau\Delta}|E_0\rangle\langle E_0| + e^{-\tau\Delta}|E_1\rangle\langle E_1|). \quad (\text{A2})$$

This implies that the ratio of probabilities for occupying the excited state $p(E_1)$ versus the ground state $p(E_0)$ is $\frac{p(E_1)}{p(E_0)} = e^{-2\tau\Delta}$ and that the shift parameter has no

effect. The value of τ to which one needs to evolve in order to obtain a good approximation to the ground state is determined by Δ , with the ground state only being well-approximated when $\tau \sim \mathcal{O}(\frac{1}{\Delta})$. For many complex systems, the low level energy states may be nearly degenerate and thus require an impractically large τ to obtain a good estimate for the ground state. If one uses any $\lambda < E_0$, however, we find

$$\frac{1}{Z} e^{-\tau(H+\lambda)^2} = \frac{1}{Z} \left(e^{2\tau\Delta(\bar{E}+\lambda)} |E_0\rangle\langle E_0| + e^{-2\tau\Delta(\bar{E}+\lambda)} |E_1\rangle\langle E_1| \right) \quad (\text{A3})$$

$$\implies \frac{p(E_1)}{p(E_0)} = e^{-4\beta\Delta(\bar{E}+\lambda)}. \quad (\text{A4})$$

The rate of convergence to the ground state with respect to τ can therefore be tuned by λ , such that the required final value is reduced by a factor of 2 ($\bar{E} + \lambda$). This phenomenon is illustrated in Fig. 8, where decreasing λ has the predicted exponential effect in the imaginary time τ_c at which $\rho^{(\lambda)}$ reaches the ground state, i.e. $|\langle H \rangle - E_0| < 10^{-4}$.

Appendix B: Additional Numerical Analyses

Here, we apply our method to compute the spectrum of a transverse-field Ising model and initialize the system in a single pure state $|\psi_0\rangle = \sum_j a_j |E_j\rangle$. Results are plotted in Fig. 9.

In this case, we specifically initialize in the all-zero state given by $|\psi_0\rangle = |0\rangle^{\otimes 8}$ is used. This implies that $\rho^{(\lambda)}(\tau)$ has the form

$$\rho^{(\lambda)}(\tau) = \sum_{ij} e^{-\frac{1}{4}\tau(E_i+E_j+2\lambda)^2} a_i a_j |E_i\rangle\langle E_j|. \quad (\text{B1})$$

Consequently, when λ is chosen such that $\langle H^{(\lambda)} \rangle(\tau \rightarrow \infty)$ converges to a band of closely spaced levels, it tends to converge towards the eigenstate corresponding to the lowest energy level in the band (i.e., rather than selecting out each level within the band separately). This occurs because of additional coherences in the energetic basis that are not present when $\rho^{(\lambda)}(0) \propto 1$, thus reinforcing the notion that it is desirable to initialize the method accordingly in the maximally mixed state.

Appendix C: Hadamard Test

Qubits are initialised in the state $|0\rangle$ before a Clifford gate is applied, in order to randomise the initial state such that over statistical sampling it mimics $\rho_S = 1$. A Hadamard gate is also applied to the ancilla qubit, such that the overall state of the system at the first barrier is

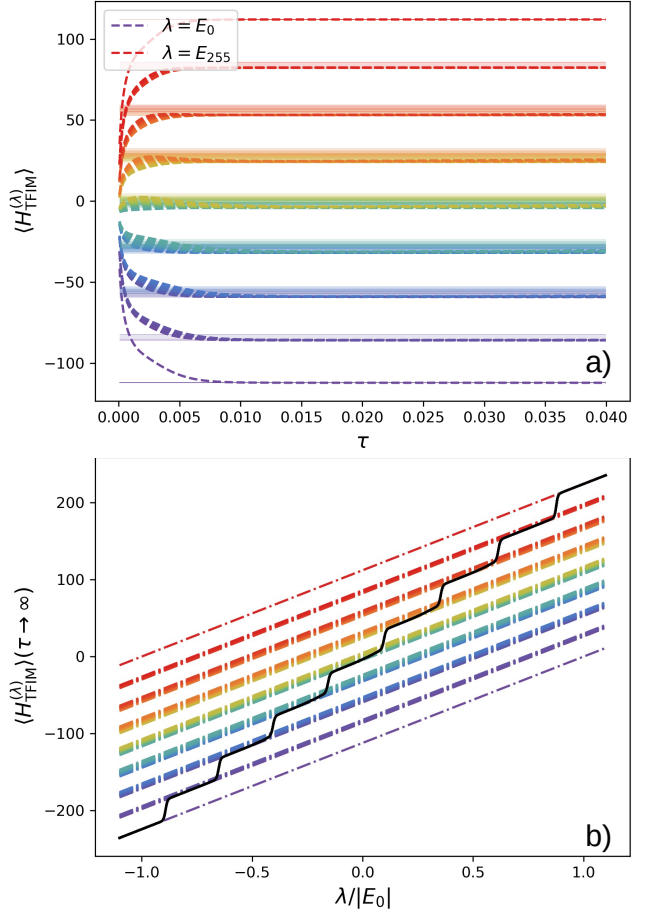


FIG. 9. Results of spectral calculations performed for an eight site Ising Hamiltonian. Dashed lines indicate the eigenenergies of H_{TFIM} . Solid lines indicate the convergence of the spectral calculation to these eigenenergies. For a), we plot the calculated energy as λ against propagation in imaginary time τ and find that our method converges to successively lower eigenstates of H_{TFIM} before reaching the ground state E_0 . For b), we plot the change in the steady state expectation value of H_{TFIM} as λ is varied, illustrating that a complete course-grained spectrum is obtainable using only expectation values estimated from a single trajectory only.

described by:

$$|\Psi_1\rangle = \frac{1}{\sqrt{2}}(|\psi_0\rangle |0\rangle + |\psi_0\rangle |1\rangle), \quad (\text{C1})$$

where $|\psi_0\rangle$ denotes the randomised initial state of our system. We then apply $2j$ copies of the unitary evolution operator \mathcal{U} to $|\psi_0\rangle$ to simulate $2j$ steps of the evolution. Each of these operators is controlled by the ancilla qubit. Then we have

$$|\Psi_2\rangle = \frac{1}{\sqrt{2}}(|\psi_0\rangle |0\rangle + \mathcal{U}^{2j} |\psi_0\rangle |1\rangle), \quad (\text{C2})$$

$$= \frac{1}{\sqrt{2}}(|\psi_0\rangle |0\rangle + |\psi_{2j}\rangle |1\rangle). \quad (\text{C3})$$

In general, one needs to decompose an observable into a series of Pauli strings so that the expectation value can be evaluated efficiently. Applying the Pauli string P_α controlled on the ancilla qubit yields

$$|\Psi_3\rangle = \frac{1}{\sqrt{2}}(|\psi_0\rangle |0\rangle + P_\alpha |\psi_{2j}\rangle |1\rangle). \quad (\text{C4})$$

Applying another $2j$ copies of \mathcal{U} controlled on the ancilla then yields

$$|\Psi_4\rangle = \frac{1}{\sqrt{2}}(|\psi_0\rangle |0\rangle + \mathcal{U}^{2j} P_\alpha |\psi_{2j}\rangle |1\rangle). \quad (\text{C5})$$

The final Hadamard acting on the ancilla mixes the superposition again to give

$$|\Psi_5\rangle = \frac{1}{2} \left(|0\rangle [|\psi_0\rangle + \mathcal{U}^{2j} P_\alpha |\psi_{2j}\rangle] \right. \quad (\text{C6})$$

$$\left. + |1\rangle [|\psi_0\rangle - \mathcal{U}^{2j} P_\alpha |\psi_{2j}\rangle] \right) \quad (\text{C7})$$

Now the probability of measuring $|0\rangle$ on the ancilla is

$$p_0 = \frac{1}{4} (\langle \psi_0 | + \langle \psi_{2j} | P_\alpha (\mathcal{U}^{2j})^\dagger) (|\psi_0\rangle + \mathcal{U}^{2j} P_\alpha |\psi_{2j}\rangle), \quad (\text{C8})$$

$$= \frac{2 + 2\text{Re}(\langle \psi_{2j} | P_k |\psi_{-2j}\rangle)}{4}. \quad (\text{C9})$$

From this, it is possible to obtain the real part of the overlap via a measurement of the ancilla, as

$$\text{Re}(\langle \psi_{2j} | P_k |\psi_{-2j}\rangle) = 2p_0 - 1. \quad (\text{C10})$$

Obtaining the imaginary part of this overlap can be achieved by modifying the circuit by applying a S gate to the ancilla between the first Hadamard gate and \mathcal{U}^{2j} gate.

Appendix D: Estimator Method

Another method of obtaining results for larger systems is to calculate the necessary overlaps directly from expectations. Explicitly, the real and imaginary parts of the overlap $\langle \psi_{2j} | O | \psi_{-2j} \rangle$ can be expressed as expectations of the Hermitian operators S_{Re}^j and S_{Im}^j i.e.

$$S_{\text{Re}}^j = \frac{1}{2} (\mathcal{U}^{2j} + (\mathcal{U}^{2j})^\dagger), \quad (\text{D1})$$

$$S_{\text{Im}}^j = \frac{1}{2i} (\mathcal{U}^{2j} - (\mathcal{U}^{2j})^\dagger), \quad (\text{D2})$$

such that

$$\text{Re/Im}(\langle \psi_{-2j} | O | \psi_{2j} \rangle) = \langle \psi_0 | O S_{\text{Re/Im}}^j | \psi_0 \rangle. \quad (\text{D3})$$

This alternative approach reduces the number of qubits used in the simulation, which reduces the errors in

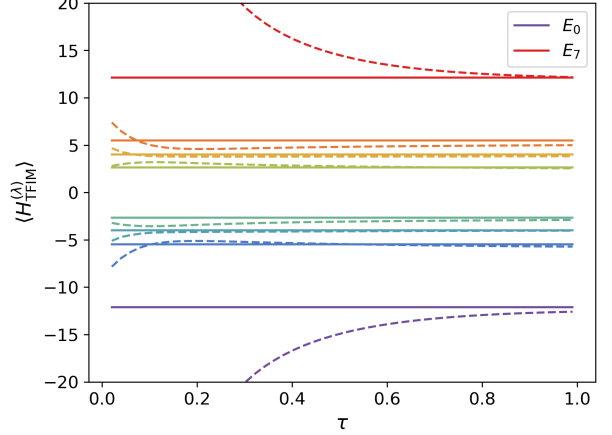


FIG. 10. Energy expectation values for a 3 site transverse field Ising model with $J = 1$, $h = 2$ as the system propagates in imaginary time obtained. The overlaps required for calculating Eqs. (32) and (33) are obtained using IBM's estimator primitive with the ibm qasm simulator to measure the expectation values of S_{Re}^j and S_{Im}^j as in Eq. (D3)

the calculation due to noisy hardware. However, this approach does not scale well in comparison to the Hadamard test approach discussed above. This is because measuring the expectation values of $S_{\text{Re/Im}}^j$ in the circuit requires decomposing \mathcal{U}^{2j} and $(\mathcal{U}^{2j})^\dagger$ into series of Pauli strings for every step. With the Hadamard test approach, we only needed to perform the Pauli string decomposition O once and then we could use it each time we evaluated the circuit. We demonstrate the utility of this approach for a 1D transverse field Ising model with $J = 1$, $h = 2$, and $L = 3$ by plotting the energy expectations against imaginary time in Fig. 10. These results are obtained using IBM's qasm simulator with the estimator primitive backend rather than a real machine. To mimic starting with the maximally mixed entangled state, we repeat the calculations with 50 different random initial states and averaging calculated overlaps at each step. These results demonstrate that the alternative approach of measuring the expectations of S_{Re}^j and S_{Im}^j can be used to calculate the energy spectrum of the system for larger systems than the Hadamard test approach for near term quantum computers.

Appendix E: Error Bounds

One may obtain an error for ITQDE by considering the continuous limit of the correspondence, namely the Hubbard-Stratonovich transformation as obtained in Sec. III. Let us evaluate the integral via Gauss-Hermite quadrature (see Eqs. (3.5.15), (3.5.19), and (3.5.28) of

Ref. [101]),

$$\begin{aligned}
& e^{-\tau H^2} \\
&= \frac{1}{\sqrt{\pi}} \sum_m \int_{-\infty}^{\infty} e^{-x^2} e^{-2i\sqrt{\tau}x E_m} |E_m\rangle \langle E_m| dx \\
&= \frac{1}{\sqrt{\pi}} \sum_m \sum_{k=1}^n w_k e^{-2i\sqrt{\tau}x_k E_m} |E_m\rangle \langle E_m| + \mathcal{E} \\
&= \frac{1}{\sqrt{\pi}} \sum_{k=1}^n w_k e^{-2i\sqrt{\tau}x_k H} + \mathcal{E}, \tag{E1}
\end{aligned}$$

where the coordinate grid $\{x_k\}$ and weights $\{w_k\}$ are tabulated in Ref. [101]. Moreover, there exists reals $\{\xi_m\}$

such that the error term is

$$\begin{aligned}
\mathcal{E} &= \frac{n!2^n}{(2n)!} (-i\sqrt{\tau})^{2n} \sum_m E_m^{2n} e^{-2i\sqrt{\tau}\xi_m E_m} |E_m\rangle \langle E_m| \\
&= \frac{n!2^n}{(2n)!} (-i\sqrt{\tau})^{2n} \sum_{m,m'} E_{m'}^{2n} e^{-2i\sqrt{\tau}\xi_m E_m} |E_m\rangle \langle E_m| \delta_{m,m'} \\
&= \frac{n!2^n}{(2n)!} (-i\sqrt{\tau})^{2n} \sum_{m,m'} E_{m'}^{2n} |E_{m'}\rangle \langle E_{m'}| e^{-2i\sqrt{\tau}\xi_m E_m} |E_m\rangle \langle E_m| \\
&= \frac{n!2^n}{(2n)!} (-i\sqrt{\tau})^{2n} H^{2n} \sum_m e^{-2i\sqrt{\tau}\xi_m E_m} |E_m\rangle \langle E_m|.
\end{aligned}$$

To write it more compactly, we can say that there is a unitary operator \mathcal{U} such that the error \mathcal{E} is

$$\mathcal{E} = \frac{n!(2\tau)^n}{(2n)!} H^{2n} \mathcal{U}. \tag{E2}$$

The error is written in the polar operator form.

From Eq. (5.6.1) of Ref. [101], we get

$$\sqrt{\frac{2\pi}{n+1}} \left(\frac{n+1}{e}\right)^{n+1} < n! < \sqrt{\frac{2\pi}{n+1}} \left(\frac{n+1}{e}\right)^{n+1} e^{\frac{1}{12n+12}}. \tag{E3}$$

Hence, for a unitary invariant matrix norm $\|\cdot\|$, we obtain the bound

$$\|\mathcal{E}\| < \frac{(n+1)^{n+1/2}}{(2n+1)^{2n+1/2}} e^{\frac{1}{12n+12}} (2\tau e)^n \|H^{2n}\|, \tag{E4}$$

which leads to

$$\|\mathcal{E}\| = \mathcal{O}\left(\left(\frac{\tau e}{2n}\right)^n \|H^{2n}\|\right), \quad n \rightarrow \infty. \tag{E5}$$